Applied Nanoscience (2019) 9:1593–1602
https://doi.org/10.1007/s13204-018-0933-3

ORIGINAL ARTICLE

The study of Fe-doped CdS nanoparticle-assisted photocatalytic degradation of organic dye in wastewater

M. Junaid[1] · M. Imran[2,3] · M. Ikram[1] · M. Naz[4] · M. Aqeel[1] · H. Afzal[1] · H. Majeed[5,6] · S. Ali[1,7]

Received: 21 November 2018 / Accepted: 7 December 2018 / Published online: 2 January 2019

Abstract

Size-tunable nanoparticles (NPs) for pristine cadmium sulfide (CdS) and iron (Fe)-doped (5, 10 and 15%) CdS were synthesized using facile chemical co-precipitation. Size-controlled NPs were prepared with thioglycolic acid (TGA) as the capping agent and their structural, optical, morphological and physiochemical evaluations were performed using X-ray diffraction (XRD), UV–visible spectroscopy, Raman spectroscopy, field emission scanning electron microscopy (FESEM) and Fourier transform infrared (FTIR). XRD revealed single cubic phase of CdS and later broader peaks upon mixing of Fe, and intensive absorption was recorded in the visible regime upon doping with redshift. FESEM confirmed spherical nanoparticles of Fe–CdS, and Cd–S linkage along with other functional groups was recognized by FTIR. $Cd_{1-x}Fe_xS$ ($x = 0$, 0.05, 0.10 and 0.15) powder was used as the photocatalyst for methylene blue (MB) degradation in visible light and catalyst in $NaBH_4$'s presence. The control CdS bleached MB faster than doped but doped CdS showed higher catalytic degradation. The Fe-doped CdS NPs showed superior catalytic potential compared to undoped CdS which suggests their use in dye industries, especially leather and tanneries. Additionally, NPs not only show superior catalytic characteristics but also help in cost reduction and complete removal of dyes for wastewater management.

Keywords Metal oxide · Graphene · Sol–gel · XRD · Photocatalytic activity

Introduction

Around 1/10th million types of dyes are produced annually and utilized in several industries such as paper, rubber, leather, textile, printing, paint, pigments and plastic (Chowdhury and Saha 2011; Shaban et al. 2018). Among these dyes, only about 10–15% of MB is discharged directly into water bodies and surrounding environment causing cancer, skin irritations, allergy, malfunctioning of liver, kidneys and reproductive system in humans (Al-Degs et al. 2008). Moreover, MB-contaminated wastewater caused severe harmful environmental issues to aquatic life with higher chemical oxygen demand (COD) (Al-Kdasi et al. 2004).

For dye removal, several techniques such as electrolysis, dialysis, ion exchange, adsorption, and photocatalytic degradation have been employed (Wang et al. 2016). However, photocatalytic degradation being environment friendly, cost effective and efficient has been utilized widely (Sivakumar et al. 2010). Semiconductor photocatalyst is preferred in dye degradation due to sustained and fundamentally applied research in environmental remediation (Chauhan et al. 2013). Fujishima and Honda (1972) reported hydrogen splitting using TiO_2 at

M. Junaid, M. Imran and M. Ikram contributed equally.

✉ M. Ikram
dr.muhammadikram@gcu.edu.pk

1 Solar Cells Applications Research Lab, Department of Physics, Government College University Lahore, Lahore, Punjab 54000, Pakistan

2 Technical Institute of Physics and Chemistry, Chinese Academy of Sciences, 29 Zhongguancun East Road, Haidian District, Beijing 100190, China

3 University of Chinese Academy of Sciences, Beijing 100049, China

4 Biochemistry Lab, Department of Chemistry, Government College University Lahore, Lahore, Punjab 54000, Pakistan

5 Department of Botany, Government College University, Lahore, Punjab 54000, Pakistan

6 Department of Food Sciences, Cholistan University of Veterinary and Animal Sciences, Bahawalpur, Punjab, Pakistan

7 Department of Physics, Riphah Institute of Computing and Applied Sciences (RICAS), Riphah International University, 14 Ali Road, Lahore, Pakistan

water expense (Su et al. 2016; Deng et al. 2017b). Transition metal sulfides (Kriegel et al. 2012; Kundu and Pradhan 2014; Ma et al. 2014; Jiang et al. 2015), metal oxides (Park et al. 2009; Xu et al. 2012; Basnet and Zhao 2016; Deng et al. 2017a), doping materials (Zhao et al. 2015; Wan et al. 2015; Deng et al. 2015), and composite heterojunctions (Dong et al. 2013; Xu et al. 2016; He et al. 2017) have been prepared to achieve efficient photocatalyst. However, metal chalcogenides have shown improved photocatalysis (Hong et al. 2014; He et al. 2016). Interestingly, cadmium sulphide (CdS) served as promising photocatalyst due to optimal band gap, ideal electronic band position, chemical and thermal stability on behalf of quantum confinement (Thambidurai et al. 2010; Wang et al. 2015). Moreover, CdS having absorbance in visible regime and its conduction band is more negative than reduction potential of H^+/H_2 (Li et al. 2008; Ertis and Boz 2017).

The CdS efficacy for photodegradation depends on the integration with suitable impurities. Transition metals (TM: Ni, Sb, Mn, Co, Fe, etc.)-doped CdS showed electrical, optical and magnetic properties as single material (Rathore et al. 2010; Kumar and Sharma 2017). Various TM-doped CdS have been synthesized but Fe doped remained less focused. Therefore, we aimed to synthesize Fe-doped CdS having all functional attributes required for efficient MB degradation. CdS size-tunable nanocrystals have been synthesized using chemical bath deposition, spray pyrolysis, laser deposition, sol–gel and successive ion layer adsorption (Mercy et al. 2014) that had some limitations. Co-precipitation being cost effective, with high doping of impurities at room temperature, adapted chemistry of doping and size control using capping agents has been utilized widely (Mercy et al. 2014). Therefore, in the current research, we aimed to prepare Fe-doped CdS using co-precipitation.

Experimental details

Materials

Cadmium chloride 2,5 hydrate ($CdCl_2$. $2{,}5H_2O$) and sodium sulfide pentahydrate ($Na_2S.5H_2O$) were acquired from "Panreac PRS" and "Daejung Chemicals and Metals Co. Ltd", respectively. For capping agent, thioglycolic acid (TGA, 80%) was purchased from "Merck". Finally, iron (III) nitrate 9-hydrate ($Fe(NO_3)_3.9H_2O$) was purchased from "UNI CHEM" and all chemicals were utilized without further processing.

Preparation of CdS and Fe doping

Chemical precipitation was adopted to synthesize CdS; 0.5 M solutions of each of $CdCl_2$, Na_2S and TGA were prepared in deionized water (DIW) under vigorous stirring for 30 min. Afterwards, TGA was added dropwise in $CdCl_2$ solution at 65 °C to control the size of nanoparticles for 15 min. Subsequently, Na_2S solution was added dropwise in $CdCl_2$ and TGA solution. The yellowish precipitates of CdS which started to form slowly were centrifuged, washed and filtered to remove all sorts of impurities. Finally, precipitates were dried at 100 °C to obtain fine powder of CdS. Later, Fe (5, 10 and 15%) was mixed in $CdCl_2$ solution for doping using the above-mentioned procedure (Fig. 1).

Photocatalytic activity process

The photodegradation activity of iron (Fe)-doped CdS NPs was evaluated in terms of photocatalytic reduction of MB (10 mg/L). A mercury (Hg) lamp (400 W) as the visible light source was used with the principal wavelength of 400–700 nm. MB (60 mL) was mixed with 10 mg suspension of the prepared photocatalyst under stirring for 5 min to achieve equilibrium between MB and nanocomposites before illumination. After exposure of visible light for specific time intervals, 5 mL suspension was collected for UV–Vis absorption to measure MB concentration. The changes in dye concentration during photodegradation were a measure of intensity of peak (665 nm) absorption with irradiation time.

Catalysis

Freshly prepared (400 µL) 0.1M sodium borohydride ($NaBH_4$) solution was mixed with 3 mL aqueous MB (10 ppm). Then 400 µL of CdS and Fe-doped CdS of certain concentration was added under agitation. The decolorization indicates reduction of dyes. However, decolorization of MB in the presence of $NaBH_4$ represents reduction of MB to leucomethylene blue (LMB) as shown in Eq. 1. The reaction without nanocatalyst was referred as blank (Fig. 2) and the absorption spectrum was determined using UV–Vis spectrophotometer (200–800 nm).

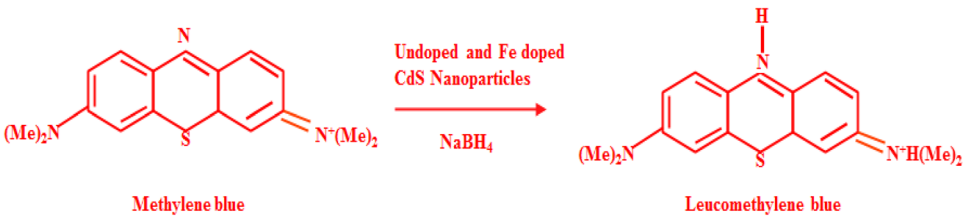

Methylene blue Leucomethylene blue (1)

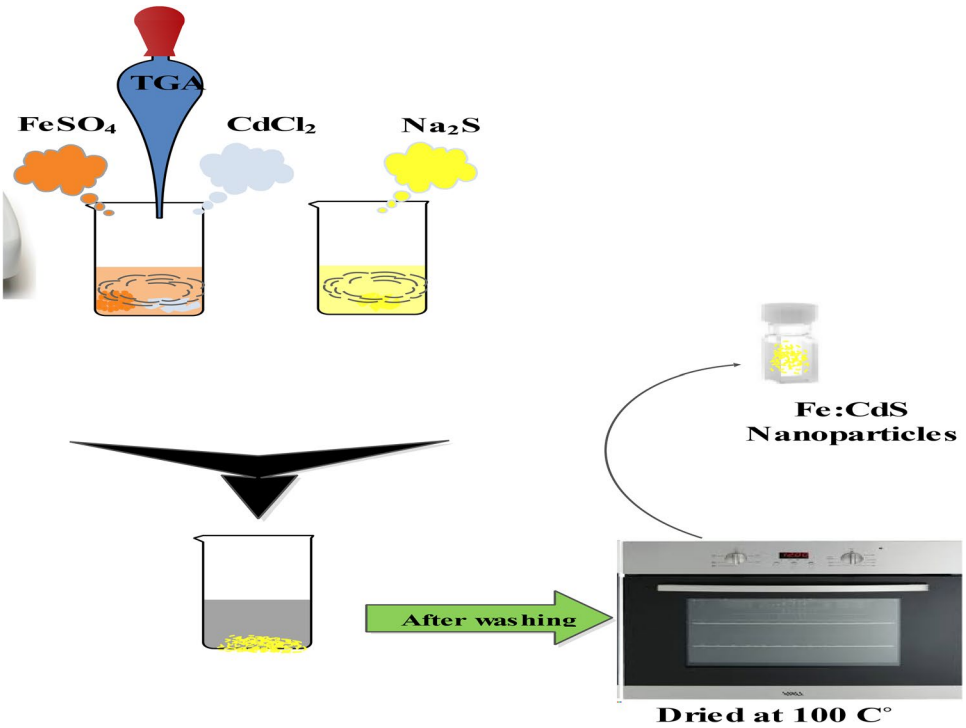

Fig. 1 Schematic representation of Fe-doped CdS preparation

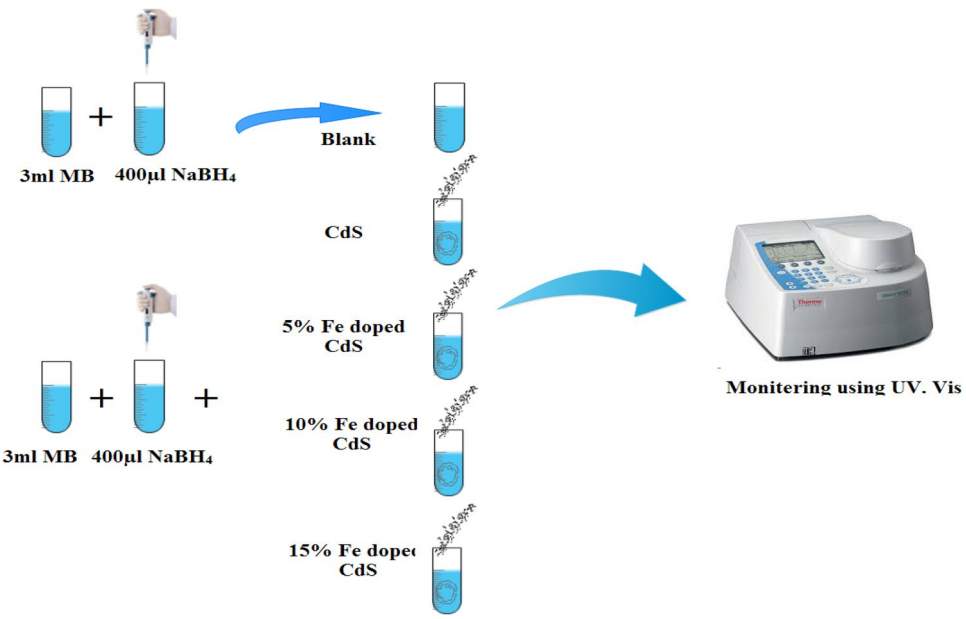

Fig. 2 Graphical representation of catalysis process

Characterization

Fe:CdS was analyzed using Fourier transform infrared (FTIR) spectroscopy, Raman spectrometer, X-ray photoelectron spectroscopy (XPS), field emission scanning electron microscopy (FESEM) and UV–Vis spectroscopy. The crystal structure of Fe-doped CdS and phase information were collected using PANalytical Xpert PRO X-ray diffraction (XRD) with Cu Kα radiation ($\lambda \sim 0.154$ nm) by varying 2θ from 20° to 70°. The presence of functional groups was confirmed using FTIR Perkin Elmer spectrometer. Raman spectra were acquired with DXR Raman microscope (Thermo Scientific) with 532-nm (6 mW) laser. The morphological characteristics and microstructures of products were investigated using JSM-6460LV FE-SEM coupled with EDX spectrometer. The optical

properties of products were obtained from UV–visible Genesys 10S spectrophotometer.

Results and discussion

Figure 3 represents the XRD pattern of $Cd_{1-x}Fe_xS$ (where $x = 0$, 0.05, 0.10 and 0.15) nanopowders that showed single cubic phase having peaks at 26.5°,43.9° and 51.9° indexed to be scattering from (111), (220) and (311) planes, respectively, and well matched with JCPDS card no. 00-001-0647. Interestingly, no extra peak appeared due to dopant material which suggests proper incorporation of Fe into CdS. The observed peaks have identical position and increased peak broadening with doping indicates surface defects and confirmed miniaturization in nanometric range for Fe–CdS NPs (Thambidurai et al. 2010). The measured average crystallite sizes were 11.6–4.1 nm using Debye–Scherrer formula $\left(D = \frac{k\lambda}{\beta \cos\theta}\right)$ from full width half maxima (FWHM) of XRD peaks, where k is Scherrer constant, λ is incident wavelength of X-rays, β is full width half maxima, θ is Bragg's angle of diffraction and D is crystallite size. The calculated crystallite size values 11.6, 11.4, 7.0 and 4.1 correspond to $x = 0$, 0.05, 0.10 and 0.15, respectively, which shows that crystallite size decreased upon Fe doping.

According to Heisenberg uncertainty principle, $\Delta X \Delta P \geq h^2/4$, which provides the relationship between particle size (ΔX) and phonon distribution momentum (ΔP), where $\hbar$ is the reduced Planck' constant. Decrease in particle size leads to increase in phonon momentum distribution that resulted in Raman band shift as well as broader peak (Chauhan et al. 2013). Raman spectra of pristine and doped CdS nanoparticles are shown in Fig. 4. Peaks at 287 and

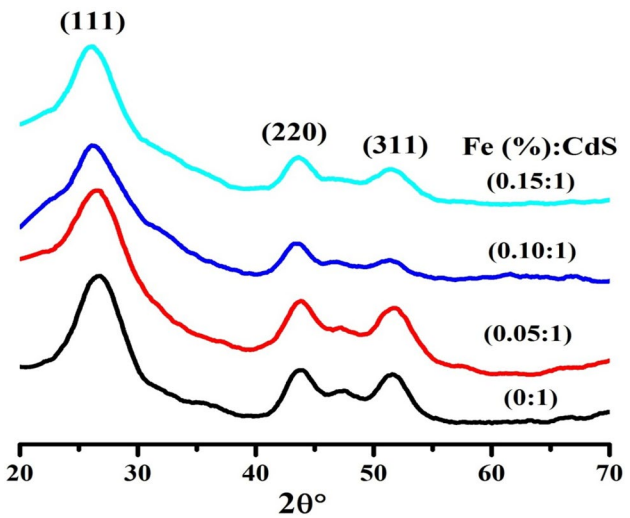

Fig. 3 XRD pattern of pristine and Fe-doped CdS

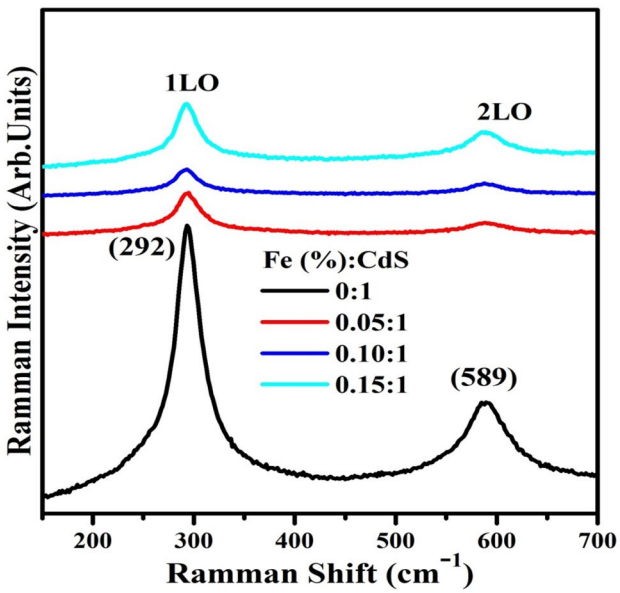

Fig. 4 Raman spectra of pure and Fe-doped CdS

589 cm^{-1} correspond to 1 LO (longitudinal optical) and 2 LO phonon modes which were consistent with previously reported values (Thambidurai et al. 2010). The peak intensity reduction upon doping attributed to the smaller difference in ionic radii of Fe^{2+} than Cd^{2+} which results in slight redshift of peaks (Chauhan et al. 2013) (Fig. 5).

The presence of functional groups was confirmed using FTIR for CdS and Fe:CdS which exhibited stretching and

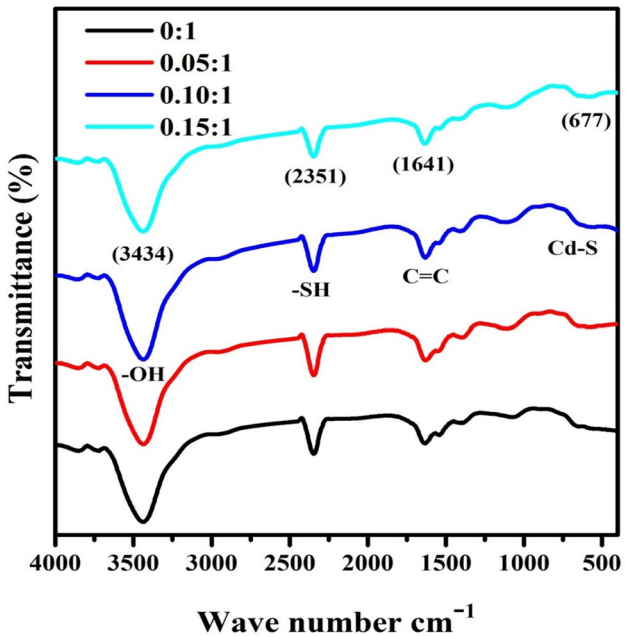

Fig. 5 FTIR spectra of CdS and Fe-doped CdS

bending vibrations of O–H, C–H, C=C and C–O functional groups. However, broad peak at 3432 cm^{-1} attributed to O–H exhibits affinity of water towards CdS (Seoudi et al. 2015; Qutub et al. 2016), whereas peaks at 1627 cm^{-1} and 1544 cm^{-1} correspond to C=C and C–O stretching modes of carboxyl and carbonyl groups (Kumar et al. 2012; Abdolahzadeh Ziabari and Ghodsi 2012; Elevathoor Vikraman et al. 2015). Interestingly, adsorption of water and CO_2 is common owing to exposure in atmosphere, particularly for NPs (Qutub et al. 2016). SH stretching vibrations were associated with an absorption band at 2351 cm^{-1} which confirmed the presence of the capping agent (TGA). However, shoulder at 665 cm^{-1} confirmed the presence of CdS stretching modes (Kumar et al. 2012; Abdolahzadeh Ziabari and Ghodsi 2012; Elevathoor Vikraman et al. 2015; Seoudi et al. 2015).

Surface morphology and elemental analysis of synthesized nanoparticles, FESEM and EDX were employed. FESEM images of synthesized CdS and Fe-doped CdS (5, 10 and 15%) NPs are shown in Fig. 6a–d, respectively. CdS had agglomerated nanoparticles (6a) that resulted in nanoclusters (Thambidurai et al. 2010). Upon doping, NPs become spherical with irregular growth due to Ostwald ripening (Devi et al. 2015; Desai et al. 2017; Waly et al. 2017). However, EDAX confirmed Cd, S and Fe (Fig. 7a–c), and the relative ratio between elements was stoichiometric (Thambidurai et al. 2010).

Optical properties after Fe incorporation into CdS (5, 10 and 15%) were investigated using UV–Vis spectroscopy (Fig. 8a). Absorption peak for CdS was found around

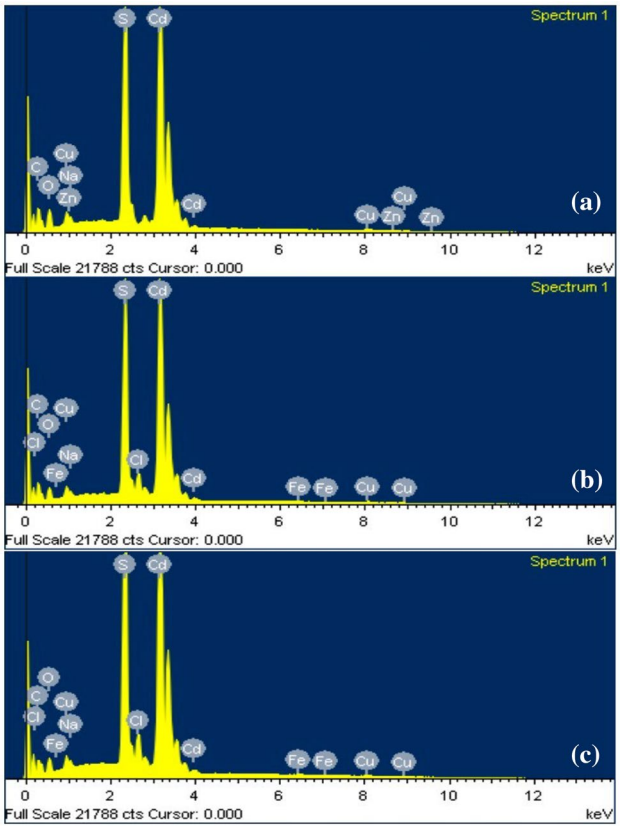

Fig. 7 EDX spectra of pristine CdS (**a**) and Fe-doped CdS (**b** and **c**)

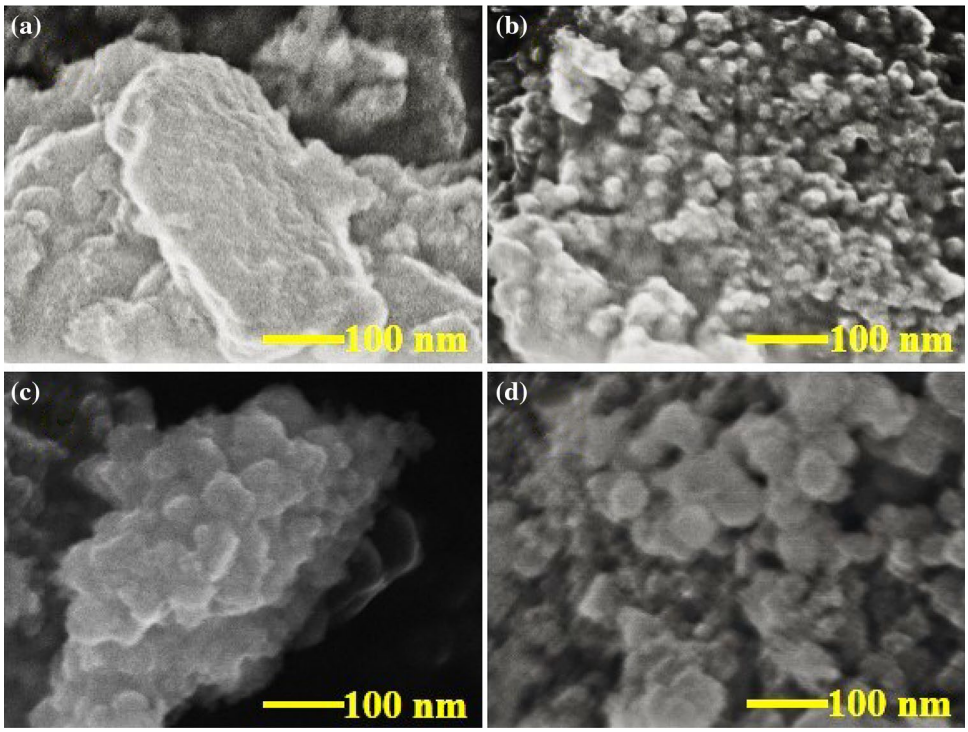

Fig. 6 FESEM images of pristine CdS (**a**) and Fe (5, 10, 15%)-doped CdS (**b, c** and **d**)

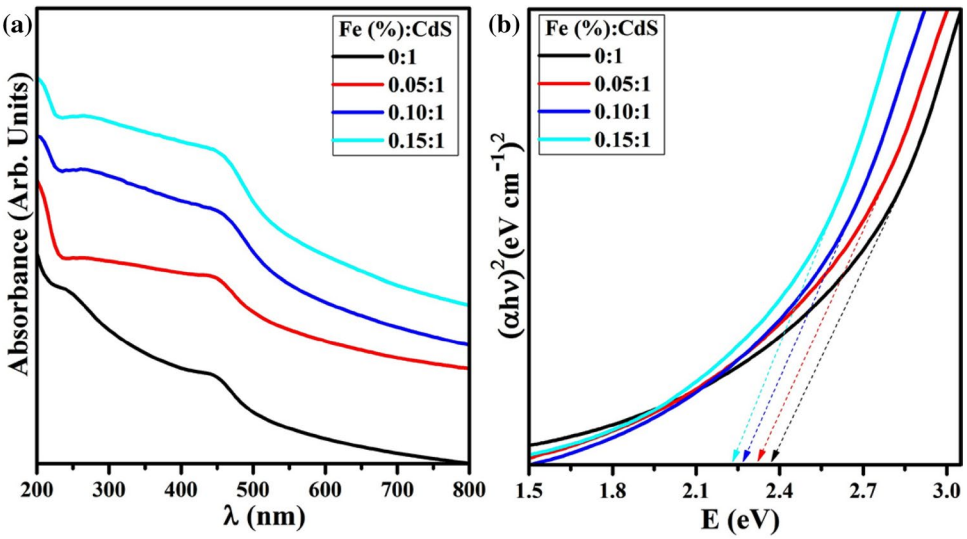

Fig. 8 Absorption and corresponding band gap spectra using Tauc plot method for pristine and Fe (5, 10 and 15%)-doped CdS

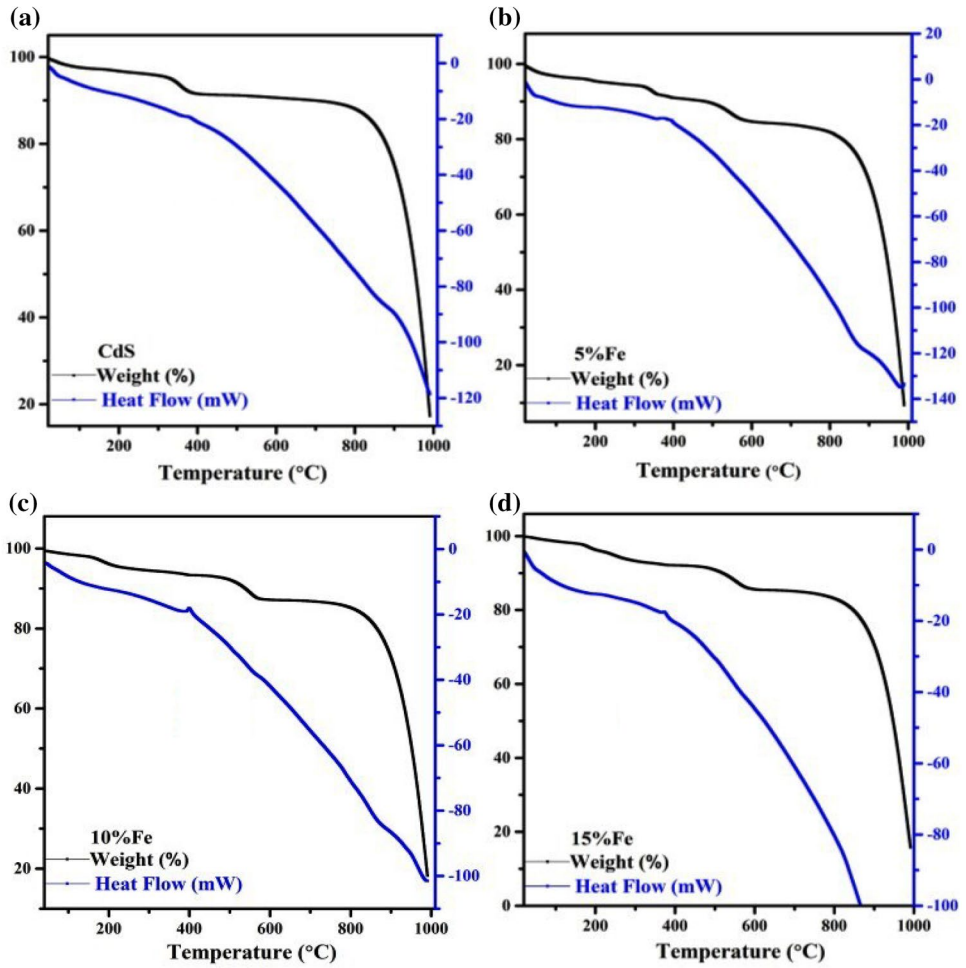

Fig. 9 DSC/TGA graph of pristine CdS (**a**) and Fe (5, 10, 15%)-doped CdS (**b, c** and **d**)

475 nm (Thambidurai et al. 2010; Seoudi et al. 2015). However, with mixing of Fe in CdS, absorption intensity increased 280–480 nm accompanied blueshift with doping amount. This shift was attributed to quantum confinement as evident from XRD (Thambidurai et al. 2010; Elevathoor Vikraman et al. 2015; Seoudi et al. 2015). On the other hand, band gap energy was measured between ($\alpha h\upsilon$) vs ($h\upsilon$) graphs plotted in Fig. 8b and longer wavelength of absorption band decreased band gap energy.

TGA analysis confirmed initial mass loss (2–10%) up to 400 °C ascribed to adsorbed water removal on nanocrystals surface for undoped and doped NPs suggesting endothermic transition as shown in Fig. 9a–d (Dhage et al. 2013; Patel et al. 2017). However, mass loss (10–30%) in doped NPs corresponds to exothermic peak that starts from 400 °C providing evidence of cubic crystal collapse and evolution of impurity phases as well (Dhage et al. 2013). Furthermore, another endothermic peak after 800 °C represented mass loss corresponding to sublimation of CdS. It is noteworthy to infer from the increase in weight loss upon Fe doping that control sample is more stable than Fe-incorporated CdS (Dhage et al. 2013) (Table 1).

The photocatalytic activity (PCA) of control and Fe-doped (5, 10 and 15%) NPs for MB degradation has been presented in Fig. 10. The successive decrease in MB with Fe-doped NPs attributed to crystal defects that acted as recombination centers to reduced photocatalytic performance. However, control sample CdS exhibited inverse degradation in contrast to doped samples (Chauhan et al. 2013).

The catalytic reduction of MB was investigated using $NaBH_4$ as the reducing agent with doped and undoped CdS as nano-catalysts. Reducing capacity of $NaBH_4$ and undoped CdS was not significant (Fig. 11a) while successive decrease in MB was observed with doping concentration of Fe in CdS and maximum catalytic efficiency was recorded for 15% Fe-doped CdS NPs (Fig. 11d).

Pure CdS gives incomplete reduction of MB within 40 min while 5% Fe-doped CdS degrades 70% MB within 25 min (Fig. 12). However, 10 and 15% Fe-doped CdS reduced MB within 15 and 10 min, respectively, and showed complete reduction of MB to leucomethylene blue (LMB) at room temperature.

The variations in absorption intensity of MB pointed to a rapid reaction rate over a certain period of time. In addition, reduction of MB was proximately completed at termination of reaction. Conversely, undoped CdS represented slower degradation of MB, suggesting superior catalytic function of Fe-doped CdS. These NPs were potential nanocatalysts with excellent catalytic potential to be employed in industries (Table 2).

Table 1 DSC/TGA result extracted from Fig. 9

Temperature range (samples)	Transition	Mass variation	Thermal behaviour
Up to 400 °C	Removal of adsorbed water	Mass loss	Endothermic
From 400 to 700 °C	Collapse of cubic structure	Mass loss	Exothermic
From 800 to 1000 °C	Sublimation of CdS	Mass loss	Endothermic

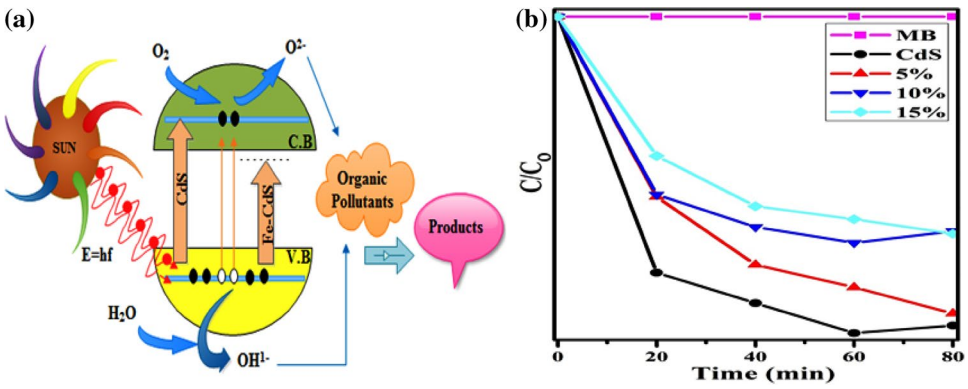

Fig. 10 Photocatalytic activity phenomena. (**a**) Degradation of MB in the presence of control and Fe-doped (5, 10 and 15%) (**b**)

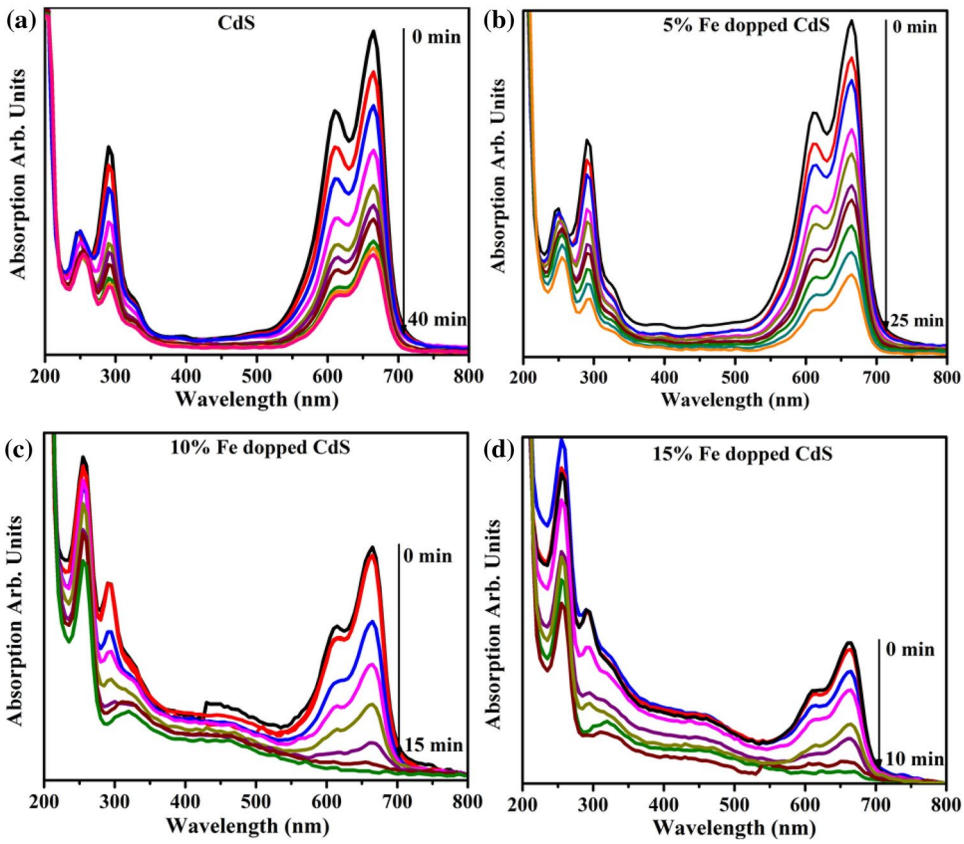

Fig. 11 **a–d** Time-dependent UV–Vis spectra for the reduction of dyes. Dye with $NaBH_4$ + CdS (**a**), dye with $NaBH_4$ + 5% Fe-doped CdS (**b**), dye with $NaBH_4$ + 10% Fe-doped CdS (**c**) and dye with $NaBH_4$ + 15% Fe-doped CdS (**d**)

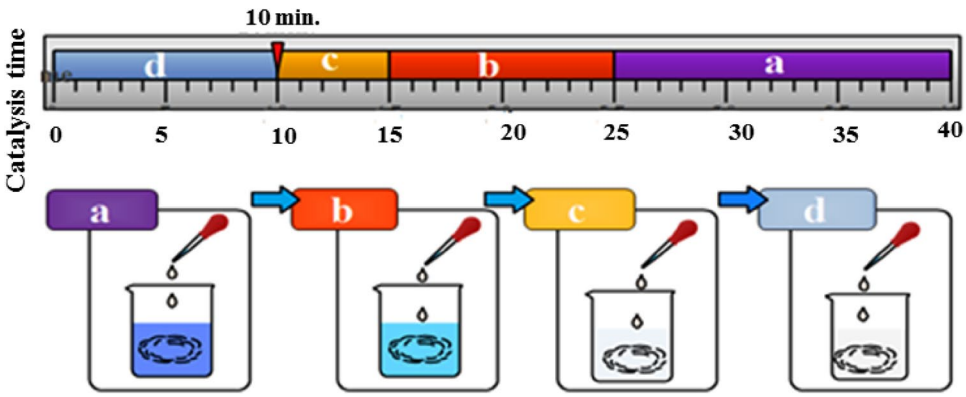

Fig. 12 Catalytic degradation of MB with CdS (**a**), 5% Fe-doped CdS (**b**), 10% Fe-doped CdS (**c**) and 15% Fe-doped CdS (**d**)

Conclusion

CdS and Fe (5, 10 and 15%)-doped CdS NPs were prepared using chemical co-precipitation and their XRD pattern indicates gradual decrease in crystallite size from 11.6 to 4.1 nm in Fe-doped CdS NPs. Absorption increased (400–500 nm) with the amount of Fe doping and bandgap decreased from 2.34 to 2.2 eV (2.42 eV of bulk CdS). FESEM images displayed nanoclusters and surface defects with doping as evident with XRD pattern. However, FTIR confirmed the presence of Cd–S linkage at 619 (cm^{-1}) and other functional groups involved during synthesis. The Fe-doped CdS NPs showed superior catalytic potential compared to undoped CdS that suggests their way to dye usage industries especially leather and tanneries. Additionally, NPs could not only provide superior catalytic activity but also help in cost reduction and complete removal of dyes for wastewater management.

Table 2 Comparison of current and reported studies of various ratios of Fe-doped CdS NPs

Reported	Fe % doped CdS	Synthesis and temperature	Particle size (nm)	Bandgap (eV)	Photocatalysis	Catalysis
Kaur et al. (2014)	0, 3, 5, 10 and 15	Solvothermal technique	7.243, 6.821, 6.495, 6.245 and 7.693	2.58, 2.59, 2.62, 2.56, and 2.55	*x*	*x*
Thambidurai et al. (2010)	1, 3 & 5	Chemical precipitation technique	2.8, 3.2, 3.8 and 4.2	Decrease in bandgap	*x*	*x*
Chauhan et al. (2013)	0, 3, 5 & 10	Chemical precipitation technique	2–3	2.3–2.2	Increase in the activity up to 3% Fe doping and then decrease up to 10%	*x*
Present Study	0, 5, 10 & 15	Chemical precipitation technique	11.6–4.4	2.4–2.1	Significant increase in the activity up to 5% upon Fe doping	Gradual increase in catalytic activity upon Fe doping

Acknowledgements This work is supported by higher education commission (HEC), Pakistan, through start research project no. 21-1669/SRGP/R&D/HEC/2017 and CAS-TWAS President's Fellowship for international PhD students, China.

Compliance with ethical standards

Conflict of interest The authors have confirmed no conflict of interest.

References

Abdolahzadeh Ziabari A, Ghodsi FE (2012) Growth, characterization and studying of sol–gel derived CdS nanoscrystalline thin films incorporated in polyethyleneglycol: effects of post-heat treatment. Sol Energy Mater Sol Cells 105:249–262. https://doi.org/10.1016/J.SOLMAT.2012.05.014

Al-Degs YS, El-Barghouthi MI, El-Sheikh AH, Walker GM (2008) Effect of solution pH, ionic strength, and temperature on adsorption behavior of reactive dyes on activated carbon. Dye Pigment 77:16–23. https://doi.org/10.1016/J.DYEPIG.2007.03.001

Al-Kdasi A, Idris A, Saed K, Teong Guan C (2004) Treatment of textile wastewater by advanced oxidation processes-a review. Glob Nest Int J 6(3):222–230

Basnet P, Zhao Y (2016) Tuning the Cu × O nanorod composition for efficient visible light induced photocatalysis. Catal Sci Technol 6:2228–2238. https://doi.org/10.1039/C5CY01464F

Chauhan R, Kumar A, Chaudhary RP (2013) Visible-light photocatalytic degradation of methylene blue with Fe doped CdS nanoparticles. Appl Surf Sci 270:655–660. https://doi.org/10.1016/J.APSUSC.2013.01.110

Chowdhury S, Saha P (2011) Adsorption kinetic modeling of safranin onto rice husk biomatrix using pseudo-first- and pseudo-second-order kinetic models: comparison of linear and non-linear methods. Clean Soil Air Water 39:274–282. https://doi.org/10.1002/clen.201000170

Deng X, Zhang Q, Zhou E et al (2015) Morphology transformation of Cu2O sub-microstructures by Sn doping for enhanced photocatalytic properties. J Alloys Compd 649:1124–1129. https://doi.org/10.1016/J.JALLCOM.2015.07.124

Deng X, Wang C, Shao M et al (2017a) Low-temperature solution synthesis of CuO/Cu_2 O nanostructures for enhanced photocatalytic activity with added H_2 O_2: synergistic effect and mechanism insight. RSC Adv 7:4329–4338. https://doi.org/10.1039/C6RA27634B

Deng X, Wang C, Yang H et al (2017b) One-pot hydrothermal synthesis of CdS decorated CuS microflower-like structures for enhanced photocatalytic properties. Sci Rep 7:3877. https://doi.org/10.1038/s41598-017-04270-y

Desai KR, Pathan AA, Bhasin CP (2017) Synthesis, characterization of cadmium sulphide nanoparticles and its application as photocatalytic degradation of congored. Int J Nanomater Chem 3:39. https://doi.org/10.18576/ijnc/030204

Devi RA, Latha M, Velumani S et al (2015) Synthesis and characterization of cadmium sulfide nanoparticles by chemical precipitation method. J Nanosci Nanotechnol 15:8434–8439

Dhage SR, Colorado HA, Hahn HT (2013) Photoluminescence properties of thermally stable highly crystalline CdS nanoparticles. Mater Res 16:504–507. https://doi.org/10.1590/S1516-14392013005000020

Dong F, Zhao Z, Xiong T et al (2013) In Situ construction of g-C_3 N_4/g-C_3 N_4 metal-free heterojunction for enhanced visible-light photocatalysis. ACS Appl Mater Interfaces 5:11392–11401. https://doi.org/10.1021/am403653a

Elevathoor Vikraman A, Rosin Jose A, Jacob M, Girish Kumar K (2015) Thioglycolic acid capped CdS quantum dots as a fluorescent probe for the nanomolar determination of dopamine. Anal Methods 7:6791–6798. https://doi.org/10.1039/C5AY01412C

Ertis IF, Boz I (2017) Synthesis and optical properties of Sb-doped CdS photocatalysts and their use in methylene blue (MB) degradation. Int J Chem React Eng 15:. https://doi.org/10.1515/ijcre-2016-0102

He J, Chen L, Yi Z-Q et al (2016) CdS nanorods coupled with WS_2 nanosheets for enhanced photocatalytic hydrogen evolution activity. Ind Eng Chem Res 55:8327–8333. https://doi.org/10.1021/acs.iecr.6b01511

He W, Wang C, Zhuge F et al (2017) Flexible and high energy density asymmetrical supercapacitors based on core/shell conducting polymer nanowires/manganese dioxide nanoflakes. Nano Energy 35:242–250. https://doi.org/10.1016/J.NANOEN.2017.03.045

Hong E, Kim D, Kim JH (2014) Heterostructured metal sulfide (ZnS–CuS–CdS) photocatalyst for high electron utilization in hydrogen production from solar water splitting. J Ind Eng Chem 20:3869–3874. https://doi.org/10.1016/J.JIEC.2013.12.092

Jiang W, Wu Z, Yue X et al (2015) Photocatalytic performance of Ag $_2$ S under irradiation with visible and near-infrared light and its mechanism of degradation. RSC Adv 5:24064–24071. https://doi.org/10.1039/C4RA15774E

Kaur K, Lotey GS, Verma NK (2014) Optical and magnetic properties of Fe-doped CdS dilute magnetic semiconducting nanorods. J Mater Sci Mater Electron 25:2605–2610. https://doi.org/10.1007/s10854-014-1918-y

Kriegel I, Jiang C, Rodríguez-Fernández J et al (2012) Tuning the excitonic and plasmonic properties of copper chalcogenide nanocrystals. J Am Chem Soc 134:1583–1590. https://doi.org/10.1021/ja207798q

Kumar S, Sharma JK (2017) Effect of nickel doping on optical properties of CdS nanoparticles synthesized via. Co-precipitation technique. Mater Sci Res India 14:05–08. https://doi.org/10.13005/msri/140102

Kumar S, Kumar S, Jain S, Verma NK (2012) Magnetic and structural characterization of transition metal co-doped CdS nanoparticles. Appl Nanosci 2:127–131. https://doi.org/10.1007/s13204-011-0046-8

Kundu J, Pradhan D (2014) Controlled synthesis and catalytic activity of copper sulfide nanostructured assemblies with different morphologies. ACS Appl Mater Interfaces 6:1823–1834. https://doi.org/10.1021/am404829g

Li K-Q, Huang F-Q, Lin X-P (2008) Pristine narrow-bandgap Sb2S3 as a high-efficiency visible-light responsive photocatalyst. Scr Mater 58:834–837. https://doi.org/10.1016/J.SCRIPTAMAT.2007.12.033

Ma L, Zhao Q, Zhang Q et al (2014) Controlled assembly of Bi_2 S_3 architectures as Schottky diode, supercapacitor electrodes and highly efficient photocatalysts. RSC Adv 4:41636–41641. https://doi.org/10.1039/C4RA07169G

Mercy A, Jesper Anandhi A, Sakthi Murugesan K et al (2014) Synthesis, structural and property studies of Ni doped cadmium sulphide quantum dots stabilized in DETA matrix. J Alloys Compd 593:213–219. https://doi.org/10.1016/J.JALLCOM.2013.12.161

Park JC, Kim J, Kwon H, Song H (2009) Gram-scale synthesis of Cu_2 O nanocubes and subsequent oxidation to CuO hollow nanostructures for lithium-ion battery anode materials. Adv Mater 21:803–807. https://doi.org/10.1002/adma.200800596

Patel NH, Deshpande MP, Chaki SH, Keharia HR (2017) Tuning of optical, thermal and antimicrobial capabilities of CdS nanoparticles with incorporated Mn prepared by chemical method. J Mater Sci Mater Electron 28:10866–10876. https://doi.org/10.1007/s10854-017-6865-y

Qutub N, Pirzada BM, Umar K, Sabir S (2016) Synthesis of CdS nanoparticles using different sulfide ion precursors: formation mechanism and photocatalytic degradation of Acid Blue-29. J Environ Chem Eng 4:808–817. https://doi.org/10.1016/J.JECE.2015.10.031

Rathore KS, Deepika, Patidar D et al (2010) Cadmium sulphide nanocrystallites: synthesis, optical and electrical studies. In: AIP conference proceedings. American Institute of Physics, pp 145–148

Seoudi R, Allehyani SHA, Said DA et al (2015) Preparation, characterization, and size control of chemically synthesized CdS nanoparticles capped with poly(ethylene glycol). J Electron Mater 44:3367–3374. https://doi.org/10.1007/s11664-015-3838-x

Shaban M, Ashraf AM, Abukhadra MR (2018) TiO2 nanoribbons/carbon nanotubes composite with enhanced photocatalytic activity; fabrication, characterization, and application. Sci Rep 8:781. https://doi.org/10.1038/s41598-018-19172-w

Sivakumar M, Towata A, Yasui K et al (2010) Dependence of sonochemical parameters on the platinization of rutile titania—an observation of a pronounced increase in photocatalytic efficiencies. Ultrason Sonochem 17:621–627. https://doi.org/10.1016/J.ULTSONCH.2009.11.013

Su J, Zhang T, Li Y et al (2016) Photocatalytic activities of copper doped cadmium sulfide microspheres prepared by a facile ultrasonic spray-pyrolysis method. Molecules 21:735. https://doi.org/10.3390/molecules21060735

Thambidurai M, Muthukumarasamy N, Agilan S et al (2010) Studies on optical absorption and structural properties of Fe doped CdS quantum dots. Solid State Sci 12:1554–1559. https://doi.org/10.1016/J.SOLIDSTATESCIENCES.2010.06.020

Waly SA, Shehata MM, Mahmoud HH (2017) Synthesis and characterization of CdS nanoparticles prepared by precipitation in the presence of span 20 as surfactant. Russ J Appl Chem 90:292–297. https://doi.org/10.1134/S1070427217020203

Wan X, Liang X, Zhang C et al (2015) Morphology controlled syntheses of Cu-doped ZnO, tubular Zn(Cu)O and Ag decorated tubular Zn(Cu)O microcrystals for photocatalysis. Chem Eng J 272:58–68. https://doi.org/10.1016/J.CEJ.2015.02.089

Wang Q, Lian J, Li J et al (2015) Highly efficient photocatalytic hydrogen production of flower-like cadmium sulfide decorated by histidine. Sci Rep 5:13593. https://doi.org/10.1038/srep13593

Wang A, Wang Y, Yu W et al (2016) TiO_2—multi-walled carbon nanotube nanocomposites: hydrothermal synthesis and temporally-dependent optical properties. RSC Adv 6:20120–20127. https://doi.org/10.1039/C5RA26677G

Xu X, Zhai T, Shao M, Huang J (2012) Anodic formation of anatase TiO2 nanotubes with rod-formed walls for photocatalysis and field emitters. Phys Chem Chem Phys 14:16371. https://doi.org/10.1039/c2cp43168h

Xu X, Gao Z, Cui Z et al (2016) Synthesis of Cu_2 O octadecahedron/TiO_2 quantum dot heterojunctions with high visible light photocatalytic activity and high stability. ACS Appl Mater Interfaces 8:91–101. https://doi.org/10.1021/acsami.5b06536

Zhao Q, Deng X, Ding M et al (2015) One-pot synthesis of Zn-doped SnO_2 nanosheet-based hierarchical architectures as a glycol gas sensor and photocatalyst. CrystEngComm 17:4394–4401. https://doi.org/10.1039/C5CE00546A

Fujishima A, Honda K (1972) Electrochemical photolysis of water at a semiconductor electrode. Nature 238:37–38